

Fabrication and packaging techniques for the application of MEMS strain sensors to wireless crack monitoring in ageing civil infrastructures

Matteo Ferri^{1*}, Fulvio Mancarella¹, Ashwin Seshia², James Ransley², Kenichi Soga², Jan Zalesky³ and Alberto Roncaglia¹

¹*Institute of Microelectronics and Microsystems (IMM), National Research Council of Italy, Via Gobetti 101, I-40129 Bologna, Italy*

²*Department of Engineering, University of Cambridge, Trumpington Street, Cambridge CB2 1PZ, UK*

³*Czech Technical University in Prague, Faculty of Civil Engineering, Thákurova 7, 166 29 Prague, Czech Republic*

(Received July 1, 2008, Accepted July 1, 2009)

Abstract. We report on the development of a new technology for the fabrication of Micro-Electro-Mechanical-System (MEMS) strain sensors to realize a novel type of crackmeter for health monitoring of ageing civil infrastructures. The fabrication of micromachined silicon MEMS sensors based on a Silicon On Insulator (SOI) technology, designed according to a Double Ended Tuning Fork (DETF) geometry is presented, using a novel process which includes a gap narrowing procedure suitable to fabricate sensors with low motional resistance. In order to employ these sensors for crack monitoring, techniques suited for bonding the MEMS sensors on a steel surface ensuring good strain transfer from steel to silicon and a packaging technique for the bonded sensors are proposed, conceived for realizing a low-power crackmeter for ageing infrastructure monitoring. Moreover, the design of a possible crackmeter geometry suited for detection of crack contraction and expansion with a resolution of 10 μm and very low power consumption requirements (potentially suitable for wireless operation) is presented. In these sensors, the small crackmeter range for the first field use is related to long-term observation on existing cracks in underground tunnel test sections.

Keywords: structural monitoring; cracks; MEMS; wireless.

1. Introduction

Crack monitoring is an important aspect in infrastructure control for collapse prevention, since sudden movements of already existing cracks are often a clear indicator of possible structure instability (Chen *et al.* 2005, Roach 2009). The best crackmeters presently available on the market are based on the vibrating wire principle. These crackmeters, whose measuring base is up to 50 cm, can be mounted across a wall crack and monitor its movement through the shift of their vibration frequency, occurring as a consequence of an applied strain, with a resolution better than 10 μE . Separate vibrating wire sensor or strain gauge can offer resolution up to 0.1 μE (Geokon Incorporated 2006).

Since their power consumption is rather high (tens of mW) these sensors are not very well suited

*Corresponding Author, Researcher, E-mail: ferri@bo.imm.cnr.it

for wireless operation, which would be extremely interesting for specific applications involving deployment of a number of crackmeters within large-scale ageing infrastructures like underground tunnels, with possibility of remote, on-demand sensor interrogation.

Through the use of silicon MEMS technology, strain sensors with high resolution, low power operation and small size can be obtained (Pisano 2007), which may represent an attractive solution for the realization of a novel crackmeter with advanced detection capabilities and possibility of wireless operation. Sensors based on MEMS oscillators, in particular, can have power consumptions in the range of 10-100 μW , provided low-power operational amplifiers are chosen to operate them in closed loop (Lee *et al.* 2008, Maxim Integrated Products 2007).

In this respect, the sensor deployment and packaging represent the main challenges, since small sensors realized on silicon chips cannot be readily applied to a wall crack. Another problem affecting the Double-Ended Tuning Fork (DETF) strain sensors proposed in the literature so far is their high motional resistance due to the width of the electrostatic gaps employed (around 2 μm), which requires the use of specially designed oscillator schemes (Wojciechowski *et al.* 2004). Packaging and bonding of the MEMS strain sensors is also an issue in their application in general (Hautamaki *et al.* 2003), and in particular concerning the problem of strain transfer from a structural material (such as steel) to the silicon substrate on which the sensors are fabricated (Sosnowchik *et al.* 2005).

In this article, possible solutions are investigated for these technical problems, aimed at realizing a crackmeter based on silicon strain sensors, including MEMS fabrication, steel bar support design and packaging solutions. In particular, section 2 reports the development of a novel technology for high-yield fabrication of DETF MEMS sensors in Silicon On Insulator (SOI) technology with submicron electrostatic gaps using a maskless line narrowing technique that can be implemented with standard near Ultra Violet (UV) lithography. Gaps scaled down to 500 nm and, consequently, DETF devices with low motional resistance have been obtained with the proposed process with good reproducibility on a 4-inch SOI substrate. Experiments concerning the implementation of a special purpose packaging method suited for applying the MEMS strain sensors to a steel bar and adhesive bonding techniques aimed at obtaining a sufficient strain transfer from steel to the bonded silicon in the crack monitoring application are described in section 3. The design of a steel crackmeter suited for the crack monitoring application with a minimum crack movement resolution of 10 μm in which the MEMS sensors and packaging techniques proposed are applied is finally described in Section 4.

2. MEMS sensors fabrication

The sensors have been designed as resonant Double Ended Tuning Fork (DETF) structures shown in schematic in Fig. 1(a). The sensor is composed by three isolated electrodes, two of which are fixed to the substrate while the third electrode is shaped in the form of a double-ended tuning fork, anchored at two ends and left free to vibrate. The device may be viewed as a two-port electrical network (Fig. 1(b)) whose transfer function presents a sharp peak located at the mechanical resonance vibration frequency of the DETF structure (see the simulation reported in Fig. 1(c)). In order to use the DETF as a strain sensor, a closed-loop operation at resonance is adopted, in which the oscillation frequency is a measure of the strain applied to the silicon substrate.

The sensors have been realized starting from boron doped SOI substrates (electrical resistivity of 1000 $\Omega\text{ cm}$ and 2000 $\Omega\text{ cm}$ for the device and handle layers respectively), composed by a 4 μm thick silicon device layer, a 1 μm thick silicon oxide layer and a 500 μm thick handle layer (Ferri *et*

al. 2008).

For the sensor fabrication, a mask set has been implemented exploring various DETF geometries. The designed devices were essentially of two types, as reported in Fig. 2.

The first geometry (Fig. 2(a)) is a DETF with parallel-plate electrode actuation, while the second one (Fig. 2(b)) utilises comb-drive electrodes. The geometrical parameters indicated in the figure have been chosen as design variables, adopting the values reported in Table 1 on different prototypes for both the parallel-plate and the comb drive devices.

The chosen geometrical parameters are related to strain resolution, resonance frequency and electromechanical impedance of the sensors. In particular, the length and width of the device (L , H) affect its mechanical resonance frequency, which is proportional to the ratio H/L , while the strain sensitivity depends on L^2/H^3 , and, consequently, is high for slender beams with large L and low H (Seshia *et al.* 2002). The width of the electrostatic gap (G) is particularly important in determining

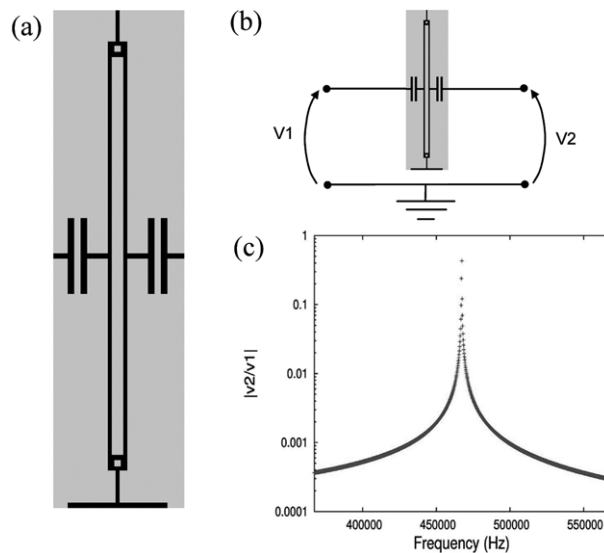


Fig. 1 (a) Resonant DETF sensor geometry, (b) two port network view of the device and (c) simulated transfer function of the two-port

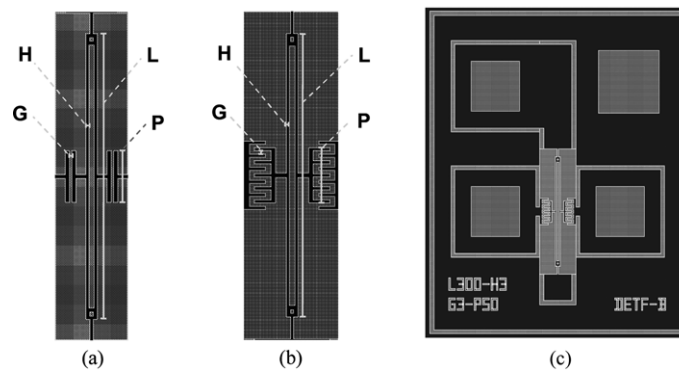


Fig. 2 (a) Parallel plate, (b) comb-drive and (c) DETF device layout and device arrangement with etching-isolated bond pads

Table 1 Design variable values of the DETF geometries on the masks

Parameter	Design variations
L	100, 300, 500 μm
G	1.25, 1.5, 1.75, 2, 2.5, 3, 4, 5 μm
H	1.25, 1.5, 1.75, 2, 2.5, 3, 4, 5 μm
P	50, 100 μm

the resonator motional resistance R_m according to the following formula (Tilmans 1997)

$$R_m = \frac{2\pi m_{eq} f_r}{Q\eta^2} \quad (1)$$

with

$$\eta = \frac{\phi_1(L/2)V_{dc}\epsilon_0 S}{G^2} \quad (2)$$

where m_{eq} is the equivalent mass of the DETF beams, f_r the mechanical resonance frequency, $\Phi_1(x)$ the eigenvalue associated with beam natural vibrations at the frequency f_r , V_{dc} the DC bias of the moving electrode, Q the resonator's quality factor, ϵ_0 the dielectric permittivity of air and S the electrode coupling surface (to a first approximation equal to $P \cdot t$, t being the device layer thickness in the process, with P defined as shown in Fig. 2). Eq. (2), in particular, holds for parallel-plate actuated devices, such as those shown in Fig. 2(a). As may be easily derived by combining Eqs. (1), (2), the motional resistance of the device turns out to be proportional to the fourth power of the coupling gap width G . Consequently, the scaling of G is a very effective way to reduce the device R_m , which has a remarkable impact on the sensor operation in closed-loop.

Devices designed with all the different geometries summarized in Table 1 have been fabricated on the same 4 inch SOI substrate. The typical arrangement of the electrodes for an individual DETF sensor (four in total, including a ground connection for the external silicon frame) is reported in Fig. 2(c). In the mask, the devices have been realized on $6 \times 6 \text{ mm}^2$ dies, including 52 dies with test structures and 120 dies with sensors prototypes (about 4300 devices on the whole wafer).

After process completion, optical microscope and SEM observation of the realized devices have been performed in order to check their release yield, and the tolerances of their geometrical features. In Fig. 3, some optical and SEM images of realized devices are provided by way of example. During the inspection, particular attention was devoted to measuring the electrode coupling gaps, whose width has been reduced using a spacer technique (Chen *et al.* 2005). As may be observed from Fig. 4, in particular, optical and SEM inspections reveal the presence of submicron gaps both on the parallel plate and comb-drive devices. This confirms the capability of the process adopted to yield submicron gaps on the actuation electrodes on the DETF devices.

As may be observed from the figure, the line narrowing technique causes the nominal lithographic gaps to shrink by roughly $1 \mu\text{m}$ (e.g., the gaps designed with an $L=1.5 \mu\text{m}$ turn out to be about $0.5 \mu\text{m}$ after the narrowing procedure, see Fig. 4). As a result, submicron gaps are obtained without resorting to costly patterning methods such as deep UV or e-beam lithography.

From the out-of-plane SEM images, the successful release of the devices has also been verified. Due to the destructive character of the SEM observation, however, optical inspection was preferred as a method to perform release yield statistics of the devices, in which particular attention was

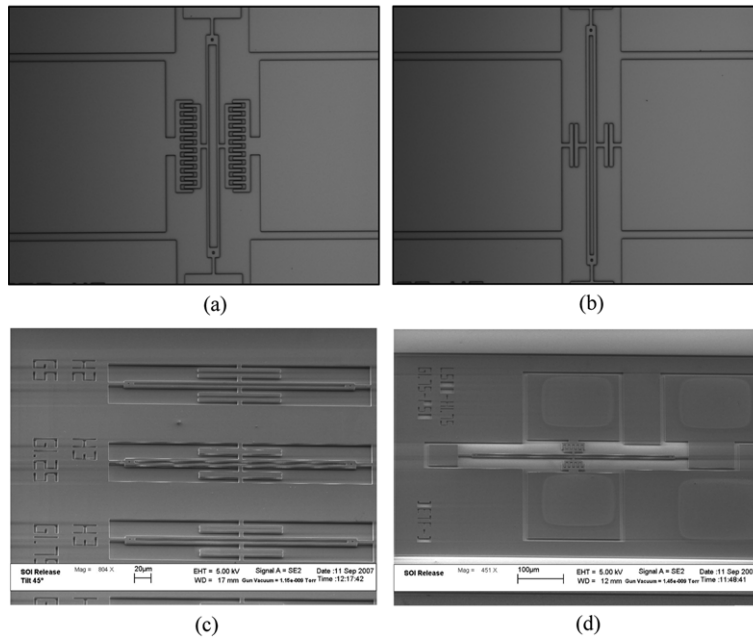


Fig. 3 Released DETFs observed at the optical and SEM microscope. (a), (d) Comb-drive and (b), (c) parallel-plate devices

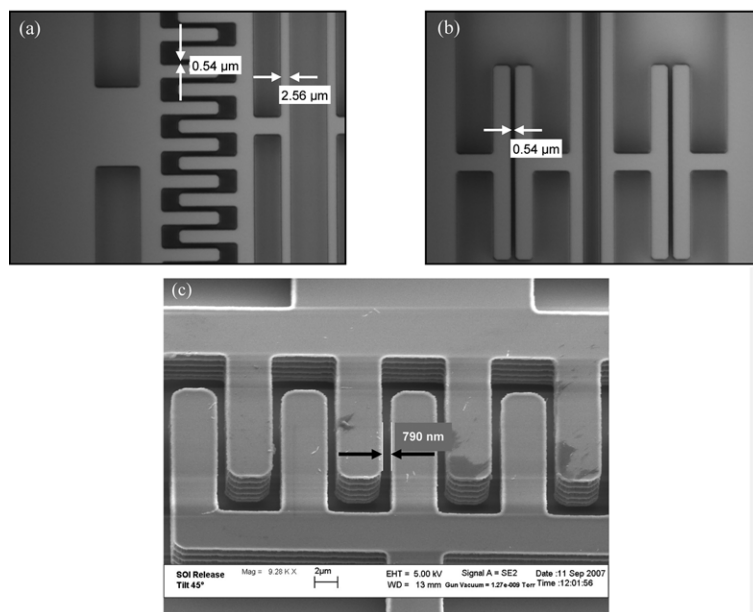


Fig. 4 Released DETFs observed at the optical and SEM microscope. (a) Comb-drive with nominal mask $L = 1.5 \mu\text{m}$, (c) $L = 1.75 \mu\text{m}$ and (b) parallel-plate device with nominal mask $L = 1.5 \mu\text{m}$

devoted to the problem of stiction.

Both vertical and lateral stiction of the devices could be clearly observed using the microscope focus at 100x magnification since, in case of stiction, the released beams were $1 \mu\text{m}$ below the anchors

Table 2 Release yield statistics of the DETF devices (performed on 16 dies)

L	Devices	Faults	Yield
100 μm	56	2	96.4 %
300 μm	279	13	95.3 %
500 μm	215	69	67.9 %
all	550	84	84.7 %

(as 1 μm is the thickness of the sacrificial oxide). By exploiting such techniques, release statistics have been performed on 16 dies on the same wafer, whose results are reported in Table 2, where the various devices are distinguished according to the double beam length (parameter L in Table 1).

As might be expected, longer devices are more prone to stiction, since they are more easily deformed by surface forces. In particular, vertical stiction is seldom observed on the 300 and 100 μm long devices, being lateral stiction or process imperfections (e.g., defects in lithography) the main causes of fault, with an overall yield above 95% in both cases. A lower yield, instead, is measured on the 500 μm long devices, mainly due to the more frequent occurrence of vertical stiction. It must be said, however, that stiction is more often observed on the dies located closer to the wafer border, while on the central dies it rarely occurs even on the longest devices. The reason for this phenomenon is not completely clear. A possible explanation could be the fact that the anti-stiction process is less effective on the wafer border, possibly depending on the sacrificial resist spinning performed before the O_2 plasma release (the process proposed in (Forsen *et al.* 2004) has been adopted). However, the overall yield of the process is very good, being around 85 % for all the devices.

From the results of the process characterization, it can be concluded that the proposed fabrication technology is suitable for fabricating DETF strain sensors with low motional resistance thanks to submicron gaps obtained with a low-cost process, employing conventional near UV lithography, with high fabrication yield.

3. Sensors packaging

In order to sense steel strain using a silicon sensor, a direct coupling between the MEMS sensor chip and the steel surface of interest is required (Hautamaki *et al.* 2003), in such a way that the strain generated on the steel body can be effectively transferred to the silicon substrate. Using conventional packaging techniques for the sensors, such coupling would be impossible since MEMS packages normally consist of plastic or ceramic boxes in which the silicon chip is enclosed and wire bonded to metal pins in order to drive the electric signals outside the package (see for instance the widely employed Dual-in-Line package (National Semiconductor Corporation 2000)). Due to the mechanical coupling needed between the bottom surface of the chip and the structural material measured (steel in this case), the use of a closed package is not possible and also the pin geometry normally implemented in standard packaging is not applicable due to geometric constraints imposed by the presence of the steel bar. In our work, a possible packaging method for silicon strain sensors on steel has been explored, ensuring effective strain transfer as well as hermeticity, robustness and possibility to provide electrical connections to a Printed Circuit Board (PCB), which is necessary to operate the sensor.

Concerning device packaging and on-field use, a possible solution has been designed according to

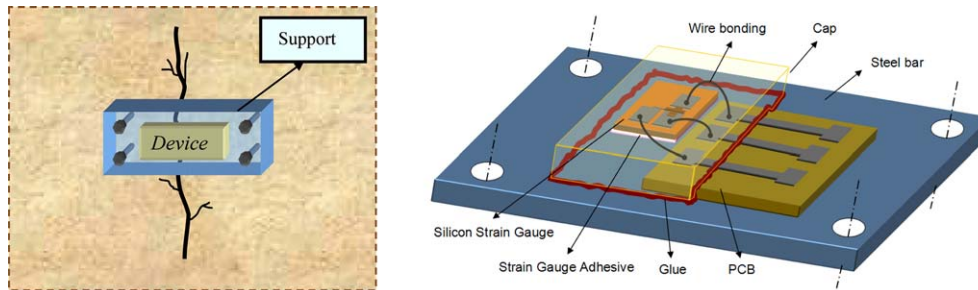


Fig. 5 MEMS strain sensor packaging scheme

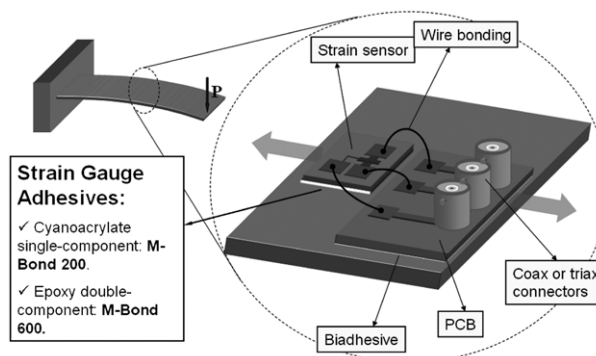


Fig. 6 Operation principle of the laboratory setup for sensors testing and calibration

the principle illustrated in Fig. 5.

The idea relies on the direct bonding of the sensors chip to a carrier steel bar, which can be fixed across a crack on a concrete wall using the conventional method used for standard vibrating wire crackmeters. On the bar, the electronics needed to operate the sensor is assembled on a PCB electrically connected to the sensor chip by standard wire bonding. In this way, the mechanical coupling between the sensor and the PCB is avoided, simplifying the strain transfer from steel to silicon. The strain gauge is bonded to the measurement bar using a cyanoacrylate or epoxy adhesive, in order to guarantee an efficient stress transfer from the bar to the sensor, while the PCB is fixed with a resin. For the on-field measurements, the strain gauge and the bond wires are encapsulated with a plastic cap glued with the same adhesive used for the sensor and sealed with polyimide for protection from the external environment (e.g., water, dust, etc.).

The described bonding and packaging methods have also been used for the laboratory tests (Fig. 6). To this purpose, a test setup consisting in a steel cantilever whose inflection can be controlled by the displacement of a precision screw at its free end has been assembled (Fig. 7). Thanks to the mechanical properties of the inflected bar (pure bending), a known strain is produced on its surface, whose value in different positions on the bar depends on the distance from the fixed end.

Using the test setup of Fig. 7, experiments have been carried out in order to determine the stress transfer from steel to bonded silicon. This investigation represents a fundamental step in determining the feasibility of the crackmeter, in which the achievement of a good strain transfer level from steel to silicon is essential. In order to do that, commercial strain sensors CEA-13-250UN-120 from Vishay (Vishay Micro-Measurements 2009) and N11-FA-03-120 from RS Components (Rsonline)

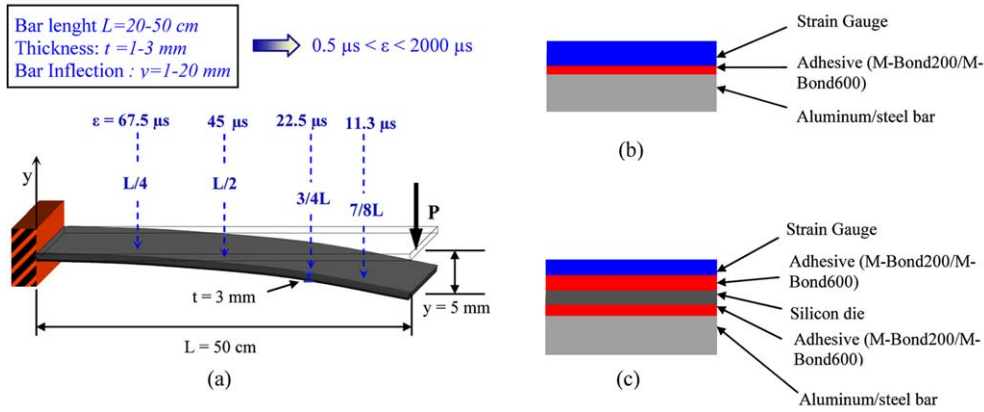


Fig. 7 (a) Stress transfer experiments performed using commercial piezoresistive strain sensors on a test bar with (b) direct coupling and (c) coupling with intermediate silicon chip

have been employed, in the two different experiments illustrated in Fig. 7.

In these experiments, the sensors have been glued on the bar using two adhesive types (both by Vishay). The first glue was M-Bond200, a two-component cyanoacrylate composite used after room-temperature curing under applied pressure. The second one was M-Bond600, a two-component epoxy that can be cured up to a temperature of 150 °C.

The first set of experiments was aimed at determining the actual strain generated by the bar at various positions from the fixed end. The measurements have been compared with the following model, derived from the theory of cantilever pure bending (Gere and Timoshenko 1997).

$$\varepsilon_x = \frac{3y_{end}t(L-x)}{2L^3} \tag{3}$$

where ε_x is the strain on the cantilever upper surface at a distance x from the clamped edge, y_{end} the deflection at the cantilever free end, t the cantilever thickness, L the cantilever length (see Fig. 10).

Eq. (3) shows that the longitudinal strain depends only on the cantilever geometry, on the deflection of

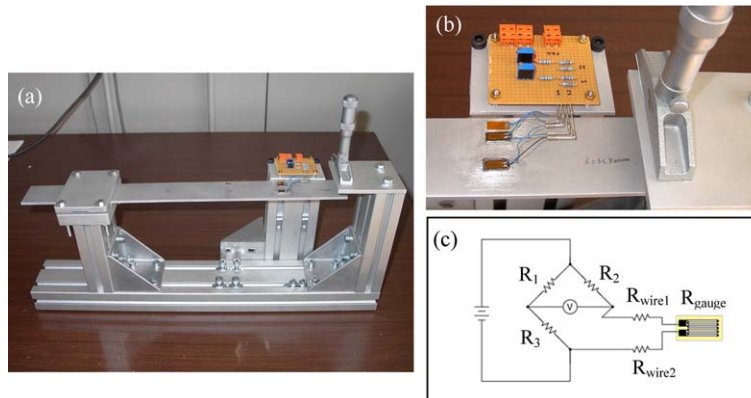


Fig. 8 (a) Inflection bar test setup, (b) detail of bonded samples with and without intermediate silicon chip and (c) Wheatstone bridge configuration employed for the sensor readout

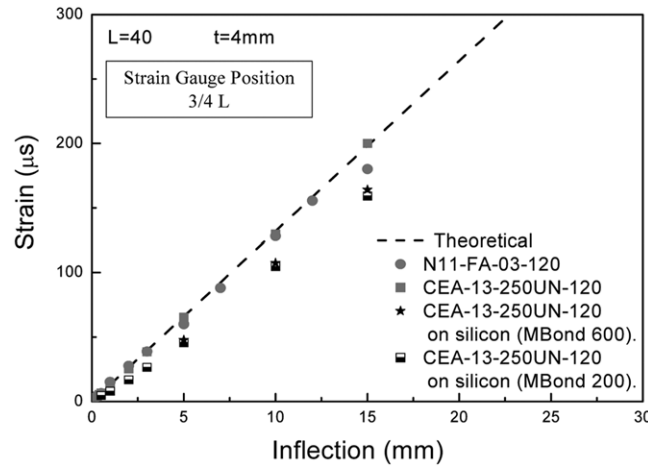


Fig. 9 Comparison between theoretical and measured strain with direct coupling (red symbols) and coupling with silicon-chip (black symbols) on the test bar

its free end and on the position along the bar.

In the experiments the commercial strain sensors, which are based on stress-induced resistance variation, have been fixed on the bar upper surface, both directly and with an intermediate silicon chip (see Figs. 7(b), (c)). After applying a controlled inflection to the bar, the sensor output has been read by means of a Wheatstone bridge for signal zeroing and temperature compensation (Fig. 8(c)), and the strain derived from the resistance-strain curve calibration provided by the supplier.

The comparison between the measurement results and the theoretical model is reported in Fig. 9, in which the measured strain at $3/4 L$ on the bar is plotted for three different cases: direct coupling of Vishay and RS type sensor, and Vishay sensor on bonded silicon chip. In the last case, the stress transfer from the steel bar to the silicon chip could be evaluated, which is of special relevance for the crackmeter application.

As may be observed in the figure, the strain transfer between the steel bar and the silicon chip bonded with glue is around 70-80%. This attenuation is most probably due to the presence of a glue layer with low Young modulus (around 2 GPa) which absorbs part of the deformation induced on the silicon chip by the steel bar bending. This attenuation is expected to be negligible on the commercial strain sensors since they are realized on polyimide, a low Young modulus material as well.

In practice, no detachment phenomena occurs during repeated deformations of the bar since the measured coupling factor turns out to be constant during different experiments and independent of the strain level. As a consequence of that, the strain measured by the sensor (ε_{Si}) can be related to the one existing on the steel surface (ε_{St}) by the formula $\varepsilon_{Si} = \alpha \varepsilon_{St}$ with α around 0.7. This means that, by performing a proper calibration, the strain measured by the MEMS sensor can be related to that produced on the steel bar by a crack movement, provided that the attenuation coefficient α is not too low compared to the sensor detection limit for ε_{Si} . For the case of resonant MEMS strain sensors, the resolution can be extremely high (strain resolutions below $1 n\varepsilon$ have been reported for silicon DETF strain sensors (Pisano 2007)), so, considering the steel bar strain levels needed for crack movement detection, an attenuation coefficient of 0.7 would not represent a significant concern for the detection of sudden changes on structure performance (such as opening of cracks). However, further improvement would be needed to reach a 100% strain transfer needed, in order to monitor the

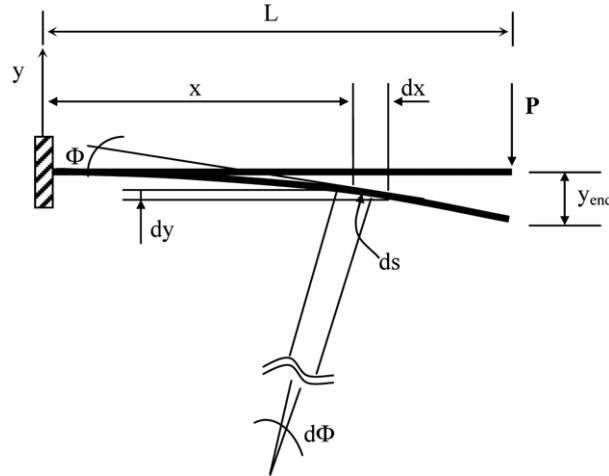


Fig. 10 Schematic representation of the cantilever deflection curve due to pure bending

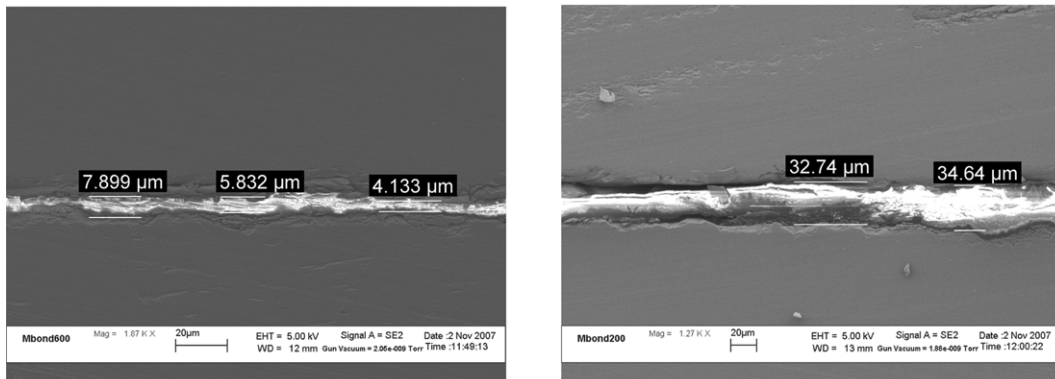


Fig. 11 SEM observation of the silicon/silicon interface with bonding glue layer for M-Bond600 (left) and M-Bond200 (right)

long-term performance of the structure. A possible way to reach this goal could be using eutectic bonding of silicon on steel (soldering) instead of adhesive bonding.

Further characterizations of the silicon/surface bonding interface have been performed by realizing cross-sections of silicon on silicon glued samples, obtained by using the same technique employed for the strain sensors of the experiments described above. These cross sections have been observed by Scanning Electron Microscope (SEM), in order to evaluate the glue layer thickness and the appearance of the silicon/glue interface (Fig. 11). The main difference observed between the two types of glue was the thickness, which is lower for the M-Bond600 (around 6-7 μm) while the M-Bond200 yields thicker layers (about 20-30 μm). However, this difference seems to have a weak effect on stress transfer (at least for the commercial strain sensors), since no relevant variations on the strain measured using different adhesives have been detected in the experiments (see again Fig. 9). The fact that the attenuation coefficient seems to be roughly the same using glues yielding layers with different thicknesses is not entirely clear, since thicker layers are in principle expected to give rise to higher attenuation. A possible explanation could be a different Young modulus of the different

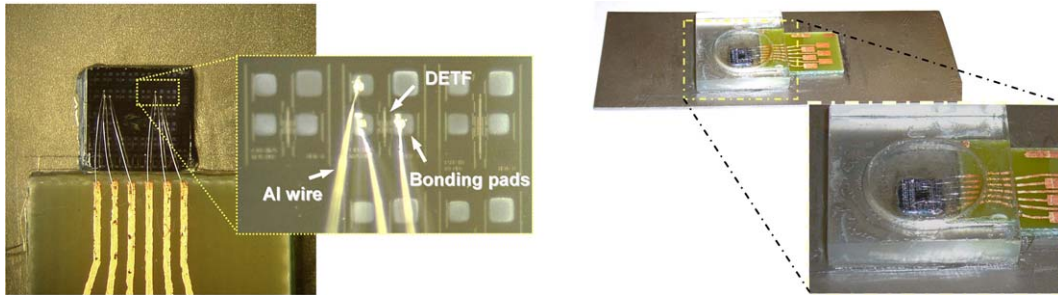


Fig. 12 Detail of direct wire bonding from the chip glued on steel bar to the PCB (left), and wire-bonded silicon chip on steel with plastic package

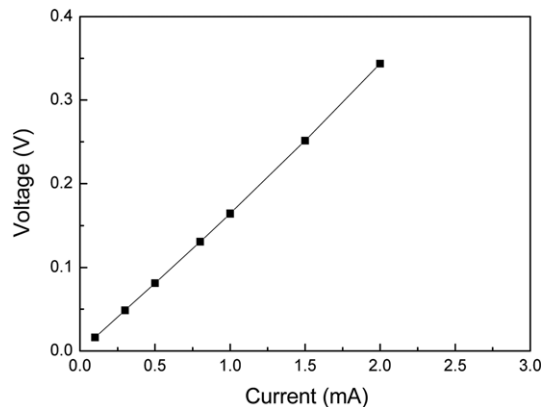


Fig. 13 Measurement of electrical connectivity on a packaged MEMS device

glues that compensates the thickness.

Direct wire bonding of silicon MEMS devices to a PCB (glued on the steel surface, as well) has also been tested for packaging. In these experiments, standard ultrasonic bonding was employed using Al/Si wires. In Fig. 12 (left), for instance, the successful bonding of two MEMS devices on a $6 \times 6 \text{ mm}^2$ chip containing the fabricated DETF sensors has been reported. The electrical connectivity between the bonded electrodes has been verified by electrical tests, with no appreciable damage of the wire bonds after the application and sealing of the cap, realized with mechanically machined plexiglass (Fig. 13). The electrical resistance of the measured connection is around 170Ω , which is largely adequate for resonant MEMS devices.

The packaging scheme shown in Fig. 12 is compatible with the adhesive bonding method shown before (the chip encapsulated of the figure was actually a strain sensor chip bonded on a steel bar). Consequently, this method can be applied to coupling and packaging of MEMS silicon strain sensors on steel surface in general and for the fabrication of a low-power steel crackmeter for ageing infrastructure monitoring in particular, according to the principle illustrated in the next section.

4. Crackmeter steel strip design

With regard to device packaging and on-field use, we expect to pre-stress the support steel strip to

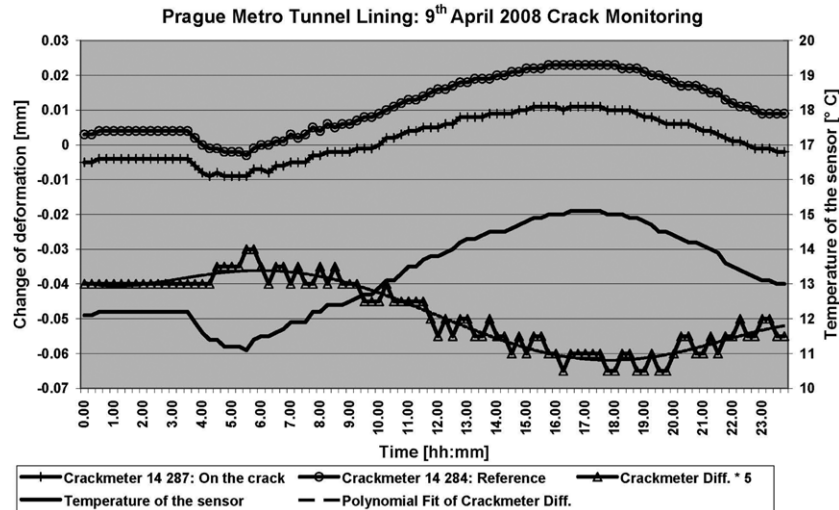


Fig. 14 Small-scale crack monitoring acquired by means of Geokon commercial crackmeters on the Prague Metro tunnel lining

measure possible crack contractions or extensions in the range (0.01-0.1 mm), with no significant tensile force applied on the crack. The range was selected with respect to pilot field use for an instrumented test section in the Prague Metro tunnel and long-term monitoring of existing cracks there. A steel strip crackmeter was designed to commence early field operation. Thermal strain is compensated with use of the strip crackmeters fitting one over the crack and the other in the intact area of the same lining element. In Fig. 14, a small range crack movement measurement performed on Prague underground tunnel lining is reported by way of example. The graph shows a time - snap of crack monitoring acquired by means of Geokon commercial crackmeters, choosing a day in which a “significant” temperature change induced a meaningful response of the crackmeters. The curve named “Crackmeter Difference” represents activity of the crack after temperature compensation and its amplitude in the graph has been multiplied by 5 for greater clarity. The same approach will be applied in case of MEMS crackmeter.

Although this measurement range can be useful in detection of very small crack movements, the sensor dynamic range would allow the detection of larger values for crack extension or contraction. In this case, however, the steel bar design presented here could be modified in order to have a less stiff tool, preventing possible mechanical solicitations of the crackmeter on the measured crack (e.g., introducing spring-like anchors and the bar ends). Also crack sliding movements could be potentially detected by means exploiting MEMS strain sensors in different directions on the chip. This application requires complete re-design of the steel strip crackmeter to transfer shear strain induced by crack sliding towards a chip with several strain sensors oriented in different directions.

In order to meet the measurement range desired for the “MEMS crackmeter”, the steel strip base length has been fixed to 200 mm. Actually, elastic range of the strip would be in this case about 0.1 mm of total extension, considering the elasticity limit of standard structural steel (0.05%). During in-field use, the strip will be pre-stressed up to 0.05 mm, leaving still 0.05 mm for the crack expansion.

Considering the elasticity modulus of structural steel ($E = 210$ GPa) of the 200 mm steel strip and at the maximum 0.05% extension, the resulting stress would be 105 MPa. With respect to selected

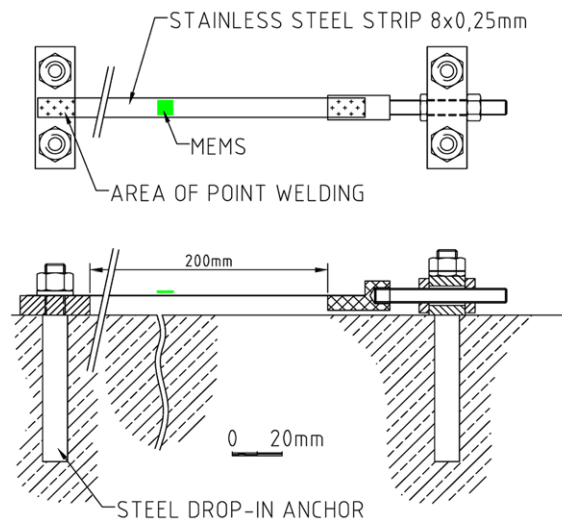


Fig. 15 Steel strip design for the MEMS-based crackmeter

sectional area of the steel strip of $8.00 \times 0.25 = 2.00 \text{ mm}^2$, the strip would force by a tension of 210 N on the crack, which should be acceptable in order to have a negligible perturbation on the crack measurement.

The extension of the steel strip base length up to 200 mm is compatible with respect to the anchors applied on a conventional crackmeter (about 320 mm). So the anchor blocks for the steel strip and the pre-stressing blocks can be placed between crackmeter anchors, realized with stainless steel.

The steel strip design is reported in Fig. 15, along with its main geometrical dimensions.

Since the proposed sensors and packaging techniques have been developed for steel surfaces, they may be also applied to other types of measurements, such as fabrication of strain gauges, load cells, pressure transducers or structural bar inflection monitoring, which could find applications in structural monitoring.

5. Conclusions

The main development steps of silicon MEMS strain sensors for the realization of a novel crackmeter suited for wireless operation in ageing civil infrastructures is reported. For the MEMS sensors, a fabrication process based on SOI technology has been presented, suited for realizing DETF sensors with electrostatic gaps scaled down to 600-800 nm, in order to ease the device operation in air. Through the use of gap narrowing techniques, the developed process allowed fabricating resonant DETF sensors with low motional resistance with no-need of expensive lithography techniques and high process yield. The silicon sensors coupling with a steel support has been investigated using adhesives normally employed for conventional piezoresistive polymer-encapsulated extensometers. The results put into evidence that an acceptable stress transfer from steel to silicon can be obtained with this technique (around 70%-80%), which is sufficient for applying the MEMS sensors to crack metering using a steel bar support with proper calibration. A special purpose packaging method has also been investigated based on direct wire bonding of the glued silicon chip on the support bar with an electronic PCB,

using a machined plexiglass cap in order to protect the sensor from the operation environment. Finally, a steel support has been designed for early field testing in order to obtain a crack extension/contraction with a resolution of 0.01 mm by applying the MEMS-based strain measurement technique described.

Further work is needed to assess the applicability of the presented crackmeter in structural monitoring, particularly on testing and validation, and possible improvements of some of the described techniques (for instance the silicon chip bonding on steel).

Acknowledgements

This work, as a part of the European Science Foundation EUROCORES Programme S3T, was supported by funds from ESF English, Spanish, Italian and Czech funding agencies and the EC 6th Framework Programme and to the Czech Science Fund supporting the project No. 103/09/1600.

References

- Chen, G., McDaniel, R., Sun, S., Pommerenke, D. and Drewniak, J. (2005), "Distributed crack sensors featuring unique memory capability for post-earthquake condition assessment of RC structures", *Smart Struct. Syst.*, **1**(2), 141-158.
- Ferri, M., Mancarella, F., Ransley, J., Yan, J., Seshia, A. and Roncaglia, A. (2008), "Fabrication of DETF sensors in SOI technology with submicron air gaps using a maskless line narrowing technique", *Proceedings of IEEE Sensors 2008*, Lecce, October.
- Forsen, E., Davis, Z.J., Dong, M., Nilsson, S.G., Montelius, L. and Boisen, A. (2004), "Dry release of suspended nanostructures", *Microelectron. Eng.*, **73-74**, 487-490.
- Geokon Incorporated (2006), <http://www.geokon.com/products/datasheets/gk403.pdf>.
- Gere, J.M. and Timoshenko, S.P. (1997), *Mechanics of materials*, 4th Ed., PWS, International Thomson Publishing, Boston.
- Hautamaki, C., Cao, L., Zhou, J., Mantell, S.C. and Kim, T.S. (2003), "Calibration of MEMS strain sensors fabricated on silicon: theory and experiments", *J. Microelectromech. S.*, **12**(5), 720-727.
- Lee, J.E.-Y., Bahreyni, B., Zhu, Y. and Seshia, A.A. (2008), "A single-crystal-silicon bulk-acoustic-mode microresonator oscillator", *IEEE Electr. Device L.*, **29**(7), 701-703.
- Maxim Integrated Products (2007), http://www.maxim-ic.com/products/amp_comp/low_power/.
- National Semiconductor Corporation (2000), http://www.national.com/ms/CE/CERAMIC_DUAL-IN-LINE_PACKAGE.pdf.
- Pisano, A. (2007), "MEMS and nano technology for the handheld, portable electronic and the automotive markets", *Proceedings of the Solid-State Sensors, Actuators and Microsystems Conference*, Lyon, France, June.
- Roach, D. (2009), "Real time crack detection using mountable comparative vacuum monitoring sensors", *Smart Struct. Syst.*, **5**(4), 317-328.
- RS Components S.P.A. (2001), <http://it.rs-online.com/web/search/searchBrowseAction.html?method=searchProducts&searchTerm=0632124&x=0&y=0>.
- Seshia, A., Palaniapan, M., Roessig, T.A., Howe, R.T., Gooch, R.W., Schimert, T.R. and Montague, S. (2002), "A vacuum packaged surface micromachined resonant accelerometer", *J. Microelectromech. S.*, **11**(6), 784-793.
- Sosnowchik, B.D., Azevedo, R.G., Cao, A., Lin, L.W. and Pisano, A.P. (2005), "Silicon-to-steel bonding using rapid thermal annealing", *IEEE T. Adv. Packaging*, **28**(4), 626-634.
- Tilmans, H.A.C. (1997), "Equivalent circuit representation of electromechanical transducers: II. Distributed-parameter systems", *J. Micromech. Microeng.*, **7**, 285-309.
- Vishay Micro-Measurements (2009), <http://www.vishay.com/strain-gages/list/product-11298/>.
- Wojciechowski, K.E., Boser, B.E. and Pisano, A.P. (2004), "A MEMS resonant strain sensor operated in air", *Proceedings of the 17th IEEE International Conference on Micro Electro Mechanical Systems (MEMS)*, 841-845.